

# Giant Gain Enhancement in Photonic Crystals with a Degenerate Band Edge

Mohamed A. K. Othman<sup>1</sup>, Farshad Yazdi<sup>1</sup>, Alex Figotin<sup>2</sup> and Filippo Capolino<sup>1</sup>

<sup>1</sup>*Department of Electrical Engineering and Computer Science, University of California, Irvine, Irvine, CA, USA. 92697*

<sup>2</sup>*Department of Mathematics, University of California, Irvine, Irvine, CA, USA 92697.*

[{mothman, fyazdi, afigotin, f.capolino}@uci.edu](mailto:{mothman, fyazdi, afigotin, f.capolino}@uci.edu)

Cavities made of photonic crystals incorporating active material have already demonstrated a stronger gain enhancement when operating at the regular band edge (RBE) of a dispersion diagram. Here instead we propose a new idea that leads to giant gain enhancement based on utilizing the unconventional slow wave resonance associated to a degenerate band edge (DBE) in the dispersion diagram of photonic crystals. We show that the gain enhancement in a Fabry-Perot cavity when operating at the DBE is several orders of magnitude stronger when compared to a cavity of the same length made of a photonic crystal with RBE. We also have found critical conditions for maximizing the total power gain. The giant gain is explained by the occurrence of a significant increase in the photon lifetime and in the local density of states. We have demonstrated DBE operated cavities that provide for superior gain conditions for lasers, quantum cascade lasers, traveling wave tubes, and distributed solid state amplifiers.

## I. INTRODUCTION

Light confinement using either mirrors or Bragg reflectors can form high quality ( $Q$ )-factor Fabry-Perot cavity (FPC) resonators with enhanced optical field intensity. Such cavities are typically used for laser applications and spectroscopy. An important class of high  $Q$ -factor structures is formed by slow-wave resonators based on the regular band edge (RBE) of the wavenumber-frequency dispersion diagram relative to photonic crystals, whose simplest architecture is a periodic stack of dielectric layers, with one dimensional periodicity [1–3]. More elaborate designs of nanocavities adopted Silicon heterostructures [4], liquid crystals [5] technologies and demonstrated improvement in the  $Q$ -factor compared to previously reported designs. The use of photonic crystals resulted in enhanced amplification properties for low-threshold lasing [2], coherent quantum electron–photon interactions [6], nonlinear optics [7] and quantum processing [8].

As proposed by Figotin and Vitebsky in [9–13], FPC resonators made of photonic crystals composed by anisotropic dielectric layers can exhibit sharp transmission peaks very close to the photonic band edge frequency. Many interesting field enhancement properties are also manifested, due to degeneracy condition of the structural eigenvalues, namely the degenerate band edge (DBE) condition. We demonstrate in this paper that based on the resonance properties discussed in [9–13], the DBE condition

leads to giant power gain when an active material is incorporated in a periodic structure. The power gain obtained can be several orders of magnitude stronger than that obtained by a comparable photonic crystal with RBE. In both cases slow-light is involved, but we demonstrate here that the DBE condition is far superior to the RBE condition for enhancing the power gain. An example of giant gain in a periodic DBE structure is clearly shown by the peak in Fig. 1 (red curve). This periodic structure is made of three layers, two anisotropic and one isotropic, exhibiting a DBE as those in [10–12], and amplification occurs when incorporating an active material. The layered stack with three different colors in the inset of Fig. 1 shows a DBE-based structure. The method used to calculate the transmission power gain is detailed in section III. The layer that includes an active material, and thus intrinsic gain, is isotropic and it can be realized by either layers of quantum wells, Raman scattering mechanisms or layers doped with active materials like Erbium, for example. A possible implementation of anisotropic layers can be carried out utilizing liquid crystals, for instance, possessing tunable anisotropic properties [5,14]. We would like to point out that the conceptual findings reported in this paper not only apply to stacks of anisotropic layers, but also to various other periodic guiding structures that exhibit the DBE condition, such as optical coupled waveguides/nanowires systems made with silicon-on-insulator technology embedded with gratings, as those in [15–17]. An attractive

application for such amplification scheme is quantum cascade lasers which are superior compared to the ones based on isotropic type of photonic crystals as in [18], with a promise of very high quantum efficiency.

## II. BACKGROUND AND METHODS

The goal of this paper is to show a possibility of giant amplification in a gain medium, that to our best knowledge have not been observed before. Such a gain medium is provided by a periodic structure supporting a DBE as we demonstrate here for a specific example based on some preliminary ideas expressed in [19]. To understand origins of the giant gain let us recall some basic properties of DBE in photonic crystals. With reference to Fig. 2(a-b) and to [9–13], we show the dispersion diagram (that relates frequency to the complex Bloch wavenumber  $k$ ) for modes associated with a specific periodic structure used in our demonstrations. (Note that in [9–13] only the real part of these Bloch wavenumbers was shown). The Bloch modes may exhibit an RBE condition at a certain frequency  $\omega_g$ . When two or more modes are allowed to propagate at the same frequency a crystal may also exhibit either a DBE at a frequency  $\omega_d$ , the split band edge (SBE) conditions. A stationary inflection point (SIP) also can be manifested in magnetic photonic crystals. Waves with  $(k, \omega)$  in the vicinity of those stationary points of the dispersion diagram exhibit almost vanishing group velocity as a consequence of multiple reflections. These waves experience an effective increase in the optical path. Indeed, the increase in the group index at an RBE condition was a basis for various studies suggesting possible gain enhancement in FPCs with RBE (see, for example, [20,21] and references therein), while the concept of SIP was investigated theoretically for unidirectional lasers [22]. The wavenumber-frequency dispersion relation for the propagating mode can be approximated by the asymptotic expression  $\Delta\omega \propto (\Delta k)^2$  near an RBE and by  $\Delta\omega \propto (\Delta k)^4$  near a DBE, where the increments are with respect to the stationary condition. We will show that this implies a gigantic increase in the density of states (electromagnetic modes) and the group index near a DBE compared to what happens near an RBE. In turn, this implies resonators  $Q$ -factors that are orders of magnitude higher than their RBE

counterparts, that scale as  $Q \sim N^5$  [10], with  $N$  being the number of unit cells of the dielectric stack.

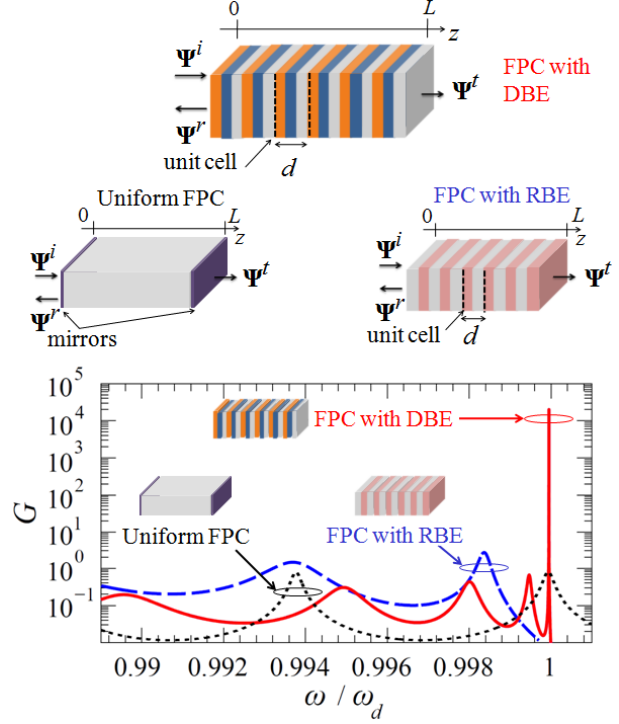


FIG. 1. Total transmission power gain  $G$  for three cavities: uniform FPC (dotted), FPCs formed by periodic structures that exhibit either an RBE for isotropic layers (dashed) or a DBE for misaligned anisotropic (birefringent) layers (solid) at  $\omega_d$ . In the top geometries, the unit cell boundaries are marked by dashed black lines. Active material is embedded in only the isotropic (gray) layers, having  $n'' = -2.2 \times 10^{-4}$ .

The  $Q$ -factor improvement in FPCs with DBE can be understood by observing a larger amount of average electromagnetic energy stored inside the resonator, compared to the energy leaking outside (when dissipation due to material losses is negligible compared to the power leaking out). In other words, the cavity effective mode volume [23] shrinks significantly close to the DBE condition, leading to high levels of field enhancement. We will quantitatively relate the enhancement of the  $Q$ -factor to the giant gain through concept of photon lifetime, in section III-B, and also to the local density of states in section V. Such intriguing features of DBE structures are investigated here can facilitate a gigantic boost in power gain, in addition to efficient manipulation of the lifetime of quantum emitters, the Purcell factors as well as nonlinear effects in DBE-based structures.

### III. GIANT GAIN AND THE WIGNER TIME INCREASE

We show in this section that the gain in an FPC operated at DBE is enhanced by several orders compared to one with an RBE condition (Fig. 1). This giant gain enhancement can be explained by a significant increase of the Wigner time compared to that for other cavities. To see that let us consider three kinds of FPCs. The first one is a conventional FPC formed by an isotropic and homogenous dielectric material bounded by two highly reflective mirrors, referred to as uniform FPC, as shown in Fig. 1. The second one is made by stacking isotropic dielectric bi-layers (referred to as FPC with RBE and shown in Fig. 1). The third one is made by stacking anisotropic tri-layers (referred to FPC with DBE) as depicted in Fig. 1, with two anisotropic layers of the same thickness  $0.31d$ , and an isotropic one of thickness  $0.38d$ , with parameters given in Appendix A. The two periodic structures have the same unit cell thickness  $d$ , and the FPC length is  $L = Nd$ . We assume that the FPC with RBE is constructed from alternating lossless dielectric layers with real refractive indices  $n_1 = 3.2$  and  $n_2 = 1.5$  with equal thickness designed to have a band edge at  $\omega_g = \omega_d$  for the sake of comparison. The uniform FPC has a refractive index of  $n = 2.25$  (see Appendix A for the case when active materials are present in these FPCs). Note that the selection of boundaries for the unit cell is depicted in the inset of Fig. 1 by dashed lines. Inside the anisotropic layers, the  $x$  and  $y$  polarizations are coupled therefore we elaborate on the electromagnetic field representation inside those layers. The guided time-harmonic electromagnetic fields (varying as  $e^{-i\omega t}$ ) along the  $z$ -direction associated to these *two* coupled waves are

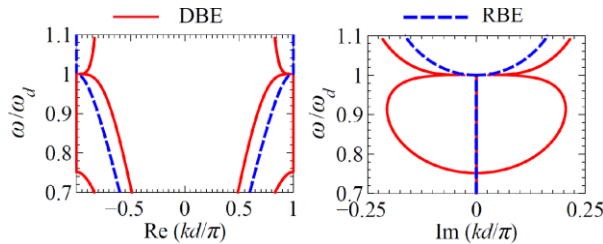


FIG. 2. Dispersion relations  $k-\omega$ , showing the real and imaginary parts of the Bloch wavenumber for the two periodic structures in the inset of Fig. 1: one that exhibits only RBE at  $\omega_d$ . (dashed) and another that exhibits DBE at  $\omega_d$  (solid).

described by a *four* dimensional state vector  $\Psi(z) = [E_x \ E_y \ H_x \ H_y]^T$ , which satisfies Maxwell's equations and boundary conditions at the interfaces between layers, and evolves along the  $z$ -direction [10,12]. The transformation across a unit cell of length  $d$  is described by using a  $4 \times 4$  transfer matrix  $\underline{T}(z+d, z)$  that relates the field between two points  $z$  and  $z+d$  as  $\Psi(z+d) = \underline{T}(z+d, z)\Psi(z)$ . Such transfer matrix is found by cascading the transfer matrices of the constitutive layers  $\underline{T}_m$  as

$$\underline{T}(z+d, z) = \prod_{m=1}^M \underline{T}_m, \text{ with } M \text{ being the number of}$$

layers per unit cell (for example  $M = 3$  for the DBE structure analyzed here, and  $M = 2$  for the RBE structure), and  $\underline{T}_m = \underline{T}_m(z+d_m, z+d_{m-1})$  where  $d_m$  is the thickness of the  $m$ th layer, and  $d_0 = 0$ . Details of calculation of such transfer matrix are presented in Appendix A. By solving the eigensystem  $\underline{T}(z+d, z)\Psi(z) = \lambda\Psi(z)$ , one obtains the eigenvalues  $\lambda$  related to the Bloch wavenumber  $k$  as  $\lambda = e^{ikd}$  that defines the modal propagation. The DBE condition is equivalent to the requirement for  $\underline{T}(z+d, z)$  to be similar to a Jordan block [10,11].

The Brillouin zone dispersion relation for the periodic structures whose unit cell defines the periodic type of FPCs is depicted in Fig. 2, showing the real and imaginary parts of the eigenmode Bloch wavenumber  $k$ . For symmetry reasons, both  $k$  and  $-k$  are modal solutions. Accordingly, the photonic crystal with pairs of isotropic layers supports only one propagating mode in the each direction below the RBE (for instance at  $\omega = 0.75\omega_g$  with  $\omega_g = \omega_d$ ).

Instead, the structure with anisotropic layers is able to support two modes simultaneously propagating in the each direction below the RBE (for instance at  $\omega = 0.75\omega_d$ ) and only one propagating mode (the other is evanescent) below the DBE at  $\omega = \omega_d$ . Just below  $\omega_d$ , there exists only one propagating mode for the RBE and DBE cases, as seen in Fig. 2. This propagating mode in the  $+z$ -direction (pertaining to the  $+k$  solution in the unbounded periodic structure) has a unique state vector denoted by  $\Psi_1$ , whose electric field components are described by the vector

$$\mathbf{E}_1 = [E_{x1} \ E_{y1}]^T.$$

For a finite stack of  $N$  unit cells as in the inset of Fig. 1 we report the exact total transmission power gain in Fig. 1 calculated as  $G = P_{\text{out}} / P_{\text{inc}}$  where  $P_{\text{inc}}$  and  $P_{\text{out}}$  are the time-average incident and transmitted power densities, respectively. We consider a transverse electromagnetic (TEM) plane wave excitation with an electric field vector  $\mathbf{E}^i$  that is polarized along the vector  $\mathbf{E}_1$ . The electric fields transmitted through the FPC comprise a vector  $\mathbf{E}^t$ , and the incident and transmitted power densities are calculated as  $\frac{1}{2}\|\mathbf{E}^i\|^2/\eta$  and  $\frac{1}{2}\|\mathbf{E}^t\|^2/\eta$ , respectively, with  $\eta$  being the wave impedance of the surrounding material, assumed to be vacuum, and  $\|\cdot\|$  represents the norm of the vector. In this example we take  $n'' = -2.2 \times 10^{-4}$  describing the isotropic active material with intrinsic gain, represented by the grey layers in the geometries in Fig. 1 (keeping the real part of their corresponding refractive indices the same as above, see Appendix A). For the DBE case the active layer is only in the isotropic region. Therefore the active material filling factor  $f$  is 100% for the uniform FPC,  $f = 50\%$  for the FPC with an RBE, and  $f = 38\%$  for the FPC with a DBE (38% is the filling factor of the isotropic layers in the FPC with DBE as explained in Appendix A), and both FPCs have  $N = 32$  unit cells. Despite the smallest active filling fraction, the structure with DBE is the one that provides giant amplification, up to four orders of magnitude larger than the FPC with RBE, as shown in Fig. 1 where we compare the total amplification provided by the structure with an RBE structure and a uniform FPC. The reasons for such giant enhancement in gain is quantified in the following section.

### A. Transmission characteristics

We calculate here the transmission coefficient  $T$  for the same stack of  $N$  unit cells shown in Fig. 1. This coefficient is polarization dependent on the impinging TEM plane wave due to the anisotropy of some layers in the FPC with DBE. We select the same incident polarization used to calculate the gain in Fig. 1, i.e., matched to the polarization state  $\mathbf{E}^i$  of the mode supported by the infinite structure. We define the transmission coefficient for FPC of length  $L$  as the projection of the transmitted electric field vector  $\mathbf{E}^t$  on  $\mathbf{E}^i$ , i.e.,  $T = (\mathbf{E}^t, \mathbf{E}^i) / \|\mathbf{E}^i\|$  where the parenthesis

denote the inner product of those two vectors in complex normed space, with  $\|\mathbf{E}^i\|$  as the norm. We observe in Fig. 3(a) a very narrow (high  $Q$ -factor) transmission peak for the FPC with a DBE, with  $N = 32$  unit cells. This occurs at an angular frequency very close and lower than to the DBE angular frequency  $\omega_d$ , because strong reflection occurs at  $\omega_d$  and for higher frequencies due to an existing bandgap [10,11]. The transmitted spectrum is densely-packed with resonances, for the FPC with DBE near the DBE frequency. By neglecting the phase shift introduced by the interfaces, the wavenumber of the DBE resonance mode for large number of unit cells  $N$  is estimated by  $k_{r,d} \approx \pi/d - \pi/(Nd)$ , and the corresponding resonance frequency  $\omega_{r,d}$  can be calculated as

$$\omega_{r,d} \approx \omega_d - \frac{b}{d^4} (\pi/N)^4 \quad [10,11] \quad \text{where}$$

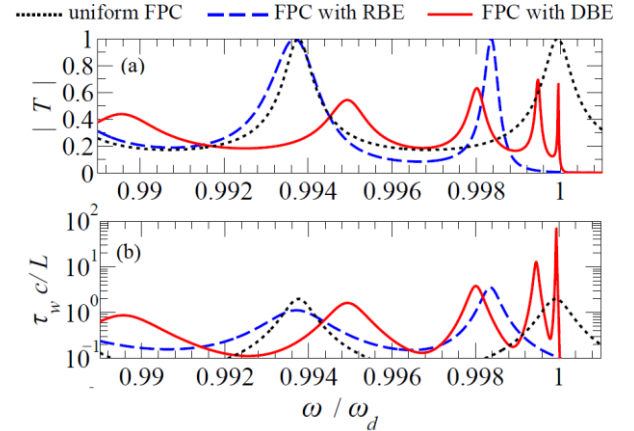


FIG. 3. (a) Magnitude of the transmission coefficient, (b) Wigner time for three types of FPCs: uniform FPC (dotted), FPCs formed by a periodic structures that exhibit either an RBE (dashed) or a DBE (solid) at  $\omega_d$ .

$b$  is a problem specific constant. For the RBE case we have a similar approximation of the resonance frequency, with  $1/N^2$  instead of  $1/N^4$  [3,20,24]. In addition, FPCs in Fig. 1, with RBE and DBE, respectively, exhibit a high quality factor resonance without using mirrors whereas the uniform FPC necessitates mirrors to reach the same quality factors of an RBE FPC cavity. Such mirrors, designed here with  $\sim 95\%$  power reflectivity can be realized by, for example, large stacks of Bragg reflectors.



## B. Wigner time and photon lifetime

Transmission properties considered in previous section are the first indicators of a possibility of enhancing gain in FPCs with a DBE. Estimation of the photon lifetime inside the FPC is yet another pass to origins of the gain enhancement. Before assessing the photon lifetime, we notice that the Wigner time of FPC (also referred to as tunneling time or group delay) is another important quantity that can be easily obtained for our structure. The Wigner time is defined as  $\tau_w(\omega) = d\varphi(\omega)/d\omega$ , where  $\varphi(\omega)$  is the total transmission phase shift accumulated across the FPC of length  $L$ , i.e., the phase of the  $T$  coefficient. As explained in [25–27], this quantity is a measure of the effective group velocity of photons passing through the FPC. Fig. 3(b) shows the normalized Wigner time for the three FPCs under study, showing more than an order of magnitude increase for the FPC with a DBE, near  $\omega_d$ . The other two types of FPCs have similar Wigner time since the resonances of those have similar  $Q$  factor for the chosen cases. Although Wigner time calculated here is based on the phase of the transmission coefficient defined previously, we have observed (not shown here) that at the DBE  $\tau_w$  becomes almost polarization independent owing to the rapid variation of the phase,  $\varphi(\omega)$  at the DBE resonance.

The Wigner time is required to calculate the effective optical path length  $L_{\text{eff}}$ , that is the length required for photons to traverse the cavity, calculated as  $L_{\text{eff}} = n_{\text{eff}}L$ , where  $n_{\text{eff}}$  is the effective group index of the cavity. Accordingly, the effective group index is given as  $n_{\text{eff}} = c\tau_w/L$  where  $c$  is the speed of light in vacuum, and  $\tau_w$  is the Wigner time of the cavity before introducing materials with intrinsic gain. The effective length,  $L_{\text{eff}} = c\tau_w$  dramatically increases near a DBE as a consequence of the Wigner time increase.

When an active material, described by complex-valued refractive index  $n = n' + in''$  with  $n'' < 0$ , is introduced in the FPC, the photon *single pass* power gain coefficient  $g_0$  of the composite medium is given by  $g_0 = \gamma Lf$ , where  $f$  is the active material filling factor in the cavity and  $\gamma$  is the per-unit-length material intrinsic gain coefficient. The latter is related in turn to the imaginary part of the wavenumber

inside that active material as  $\gamma = -2k_0 n''$  with  $k_0 = \omega/c$  [25,26]. We define then an effective gain coefficient  $g_{\text{eff}}$  as the gain experienced by photons traveling through the FP cavity, that is

$$g_{\text{eff}} = g_0 L_{\text{eff}} / L = g_0 n_{\text{eff}} = \gamma f c \tau_w. \quad (1)$$

This reveals that the effective gain coefficient of an FPC is the product of the intrinsic material gain coefficient and the FPC Wigner time. The above formula is valid provided that  $\gamma$  is sufficiently small not to deteriorate the modal properties of the DBE resonance, as discussed in the following section. Notice also that the transmission power gain in general is polarization dependent, and there exists specific polarizations maximizing the gain. However, it is the Wigner time that is a decisive factor for the giant power gain enhancement with far more significant impact on the power gain than the incident polarization. The total power gain  $G$  at a DBE resonance can be estimated using the effective gain coefficient, as follows. Let us denote  $G_{\text{approx}}$  as an estimate of the exact total power calculated as  $G_{\text{approx}} = |T|^2 e^{g_{\text{eff}}}$  at resonance. This is a simple way to approximate the small-signal amplifier transmission power gain from the transmission and gain coefficients. Note that the scaling with the transmission coefficient is necessary here to obtain an estimate of the total power transmission gain  $G_{\text{approx}}$ , since  $|T| \neq 1$  at a DBE resonance as seen in Fig. 3. In section V we quantify and compare an estimate of the total power gain using such formula and the power gain shown in Fig. 1. When conceiving structures with large effective gain coefficient one has to keep in mind that its dependence on the cavity and material properties as described by formula (1), cannot hold if the resonance is largely perturbed as discussed in the next section.

It is also instructive to compare the Wigner time with the concept of photon lifetime  $\tau_c$ , which is the time it takes the stored energy to decays to  $1/e$  of its original value due to dissipation. Such a quantity is frequently used in laser physics to express the resonator finesse [25,27,26] as well as to provide a good estimation of the Wigner time, as explained in many different situations [24,28–32]. Although lifetime and group delay are different concepts, they are intimately related. Indeed, for a uniform lossless

FPC at resonance we have an exact identity  $\tau_c = \tau_w$  [30,32], which means that stored energy lifetime in such cavity identically equals to the time it takes the wave packet to traverse the whole FPC [32], but this identity is not exactly satisfied in general. The importance of  $\tau_c$  relies in its explicit link to the  $Q$ -factor via  $Q = \omega\tau_c$  [27,26], whereas there exist approximations of the  $Q$  factor using the Wigner time [29]. The lifetime quantifies the evolution of energy with time inside the FPC. Near the DBE,  $\tau_c$  is extremely large because the quality factor is enhanced [10,13] leading to eminently high levels of stored energy. This may have impacts on significantly lowering the lasing threshold condition in laser devices.

#### IV. CRITICAL GAIN CONDITION

Since DBE is a precise mathematical condition, i.e., it only emerges when the transfer matrix becomes similar to a Jordan Block, a large amount of extrinsic perturbation (active material with  $n'' < 0$ ) can eventually deteriorate this condition. To put things into perspective, large single pass gain  $g_0$  can deteriorate the slow-wave phenomena condition associated with the DBE implying that large enhancement of photon lifetime would not occur anymore. On the other hand usually very small single pass gain  $g_0$  will not result in a strong amplification [21]. Therefore, one may expect that there exist an optimum amount of active material filling, large enough to surpass losses in the FPC but small enough not to significantly perturb the DBE condition, hence resulting in maximized amplification. This can be seen in Fig. 4(a-b) where we show the power transmission gain  $G$  varying the imaginary part of the refractive index  $n''$  (which may be a result of tuning the pump power or volume concentration of active material). We observe for such a FPC, operating near the DBE, the existence of an optimum amount of material gain to achieve the maximum amplification  $G$ . For instance for  $N=30$  unit cells the maximum power gain  $G_{\max}$  is  $10^4$ , relative to an optimum  $n'' \cong -6 \times 10^{-4}$ , whereas when  $N = 50$  the maximum is  $3 \times 10^5$  relative to an optimum  $n'' \cong -5 \times 10^{-5}$ . Therefore a careful selection of the intrinsic gain distribution inside the FPC may result in large amplification (due to better field

enhancement and localization) with even less single pass intrinsic gain, leading to a higher power conversion efficiency in laser amplifiers. Note that for simplicity, gain saturation effects and lasing line shapes are ignored in this study since we deal with a narrow band phenomenon whose bandwidth is in general much smaller than the laser line shape for homogenous broadening mechanisms. Furthermore, gain saturation that is a result of nonlinear effects is important when dealing with laser oscillators which will be subject of a future investigation, whereas in this premise we study small signal, linear giant amplification regimes.

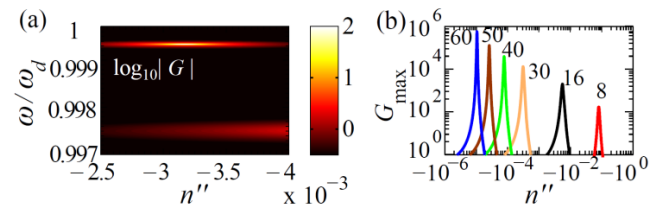


FIG. 4. (a) Plot of total power gain  $G$  varying as a function of frequency and the material gain  $n''$  around the DBE frequency for an FPC with DBE, with  $N = 16$ . (b) Maximum power gain  $G$  achieved and the optimum values of  $n''$ , for different number of layers  $N$  indicated by the numbers.

#### V. GIANT ENHANCEMENT OF LOCAL DENSITY OF STATES

As a final step toward providing a comprehensive picture of the modal properties of an FPC with DBE that contribute to giant gain, we investigate the local density of states (LDOS) inside the FPC with DBE. Fermi's golden rule states that emitters' decay rates are proportional to the LDOS in an open resonator [6,23,33]. The emitter is modeled as an electric sheet current source with the current density of the form  $\mathbf{J} = J_0 \hat{\mathbf{p}} \delta(z - z')$ , where  $\hat{\mathbf{p}}$  is a transverse unit vector with  $\hat{\mathbf{z}} \cdot \hat{\mathbf{p}} = 0$ , and consequently only transverse-to- $z$  electromagnetic waves contribute to the LDOS in this case for consistency (see Appendix B for details). We are interested in the average of the projected (or partial) LDOS  $\rho(\hat{\mathbf{p}}, z)$  over all possible orientations  $\hat{\mathbf{p}}$ . Accordingly, the average  $z$ -dependent LDOS  $\rho(z)$  in an open, lossless FPC is proportional to the trace of the  $2 \times 2$  dyadic Green's function  $\underline{\underline{\mathbf{G}}}(z, z)$  and given by [33–36]

$$\rho(z) = \langle \rho(\hat{\mathbf{p}}, z) \rangle_{\hat{\mathbf{p}}} = -\frac{k_0}{\pi c} \text{Im} \left( \text{Tr} \left[ \underline{\underline{\mathbf{G}}}(z, z) \right] \right), \quad (2)$$

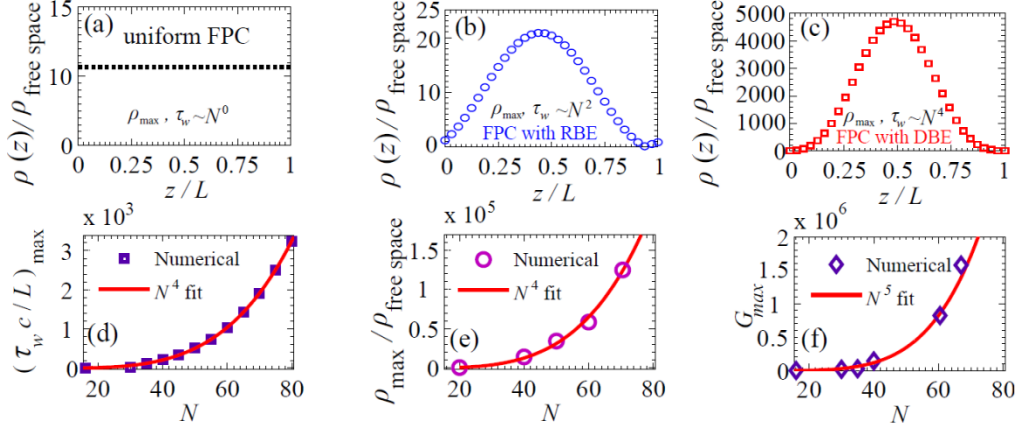


FIG. 5. Sampled local density of states (LDOS) normalized by the LDOS in free space inside (a) uniform FPC sampled at maxima locations, (b) FPC with RBE and (c) FPC with DBE sampled at points  $z = md$ ,  $m = 0, 1, 2, \dots, N$  with  $N = 32$ . (d-e) Trend of the Wigner time and LDOS varying the number of unit cells  $N$  showing an accurate fit to  $N^4$ , and (f) is the trend of the maximum achievable power transmission gain fitted to  $N^5$ .

where Im and Tr denote respectively the imaginary part and the trace, and  $\langle \cdot \rangle_{\hat{\mathbf{p}}}$  denotes the average over all possible emitter polarization directions. We construct then  $2 \times 2$  matrix (dyadic) Green's function  $\underline{\underline{\mathbf{G}}}(z, z)$  that provides transverse electric field response to a Dirac delta sheet current polarized in  $x$  and/or  $y$  directions at  $z = \text{constant}$ . The precise definition of  $\underline{\underline{\mathbf{G}}}(z, z)$  and its properties are given in Appendix B. For the particular case where a DBE is occurring, we apply the transfer matrix formalism, analogously to what was done in [24,37,38] for a simpler photonic crystal made by a stack of isotropic layers as detailed in Appendix B. We report in Fig. 5(a-c) the LDOS normalized by the LDOS in free space for the three types of FPCs considered in this paper. For simplicity the LDOS is sampled once per unit cell in the two periodic structures (those with RBE and DBE) since it varies also within each unit cell. We observe that the LDOS for the FPC with DBE or with RBE peaks around the cavity center. Vice versa the uniform FPC has a uniform LDOS envelope across the length, when evaluated as sampling the LDOS at each maximum of the electric field and the envelope is independent on the resonant mode; only the number of maxima depends on the chosen resonance.

The largest LDOS enhancement occurs for the DBE case, and it is due to the unconventional DBE resonance inside the cavity that generates giant fields.

These giant fields are caused by a strong excitation of both propagating and evanescent modes in the FPC, as a necessity to satisfy the boundary condition at the FPC edges. There, the continuity of the tangential fields to match the outside field is obtained by destructive interference between intense propagating and evanescent internal modes. Toward the center of the cavity the evanescent modes are not present anymore, and the absence of destructive interference leaves the propagating modes with giant intensity, as explained in details in [10,11]. The LDOS enhancement up to two orders of magnitude is considered a remarkable property that indeed relates to the giant amplification regimes, as described next. As shown in [25] the Wigner time  $\tau_w$  is proportional to the spatial average of LDOS over the length of the cavity  $\langle \rho(z) \rangle_L$ , where the brackets denote a spatial average over the length  $L$ . In other words, we may write  $\tau_w = K \langle \rho(z) \rangle_L$  where  $K$  is a constant, that is a function of the dielectric contrast of the layers [24]. (A detailed analysis of how determining the constant  $K$  is outside the scope of this paper, however it can be developed following the procedure detailed in [24]). It is important to note that the effective gain coefficient  $g_{\text{eff}}$  in (1) is in turn proportional to the average of the LDOS and we can also write the gain coefficient enhancement factor as proportional to the ratio between LDOS to that in free space

$$g_{\text{eff}} = g_0 \frac{c\tau_w}{L} = g_0 \frac{\langle \rho(z) \rangle_L}{\rho_{\text{free space}}} K, \quad (3)$$

where  $\rho_{\text{free space}} = 1/(\pi c)$ . In our case we evaluate  $K$  as  $K = \langle \rho(z) \rangle_L / \tau_w$ , which leads to  $K = 0.045$  at the DBE resonance. Accordingly, we compare the total power transmission gain  $G$  calculated in Fig. 1 at the DBE resonance, as ratio of transmitted and incident fields, and the one estimated by either (1) or (3) as

$$G_{\text{approx}} = |T|^2 e^{g_{\text{eff}}}, \quad (4)$$

where the transmission coefficient  $T$  is evaluated for the structure without gain (Fig. 3(a)). The total transmission gain  $G$  calculated at the DBE resonance in Fig. 1 as field ratio at its peak is  $G \cong 2 \times 10^4$ , while using the latter approximate formula leads to a peak  $G_{\text{approx}} \cong 2.015 \times 10^4$ , when considering  $g_0 = 0.11$  based on the value of  $n'' = -2.2 \times 10^{-4}$  that in turns results in  $g_{\text{eff}} \cong 10.7$ . This indicates an evident agreement between the exact gain and the estimation using the LDOS or Wigner time in (4), and proves that the giant gain enhancement is intimately related to the giant boost in Wigner time and LDOS.

Finally, we investigate the gigantic scaling of gain, Wigner time and LDOS with the cavity length. First of all, increasing the number of unit cells, or equivalently the cavity size  $L$ , will increase the effective gain coefficient  $g_{\text{eff}}$  (and hence the total power gain  $G$ ), quality factor, and LDOS for an FPC. However, for a uniform cavity those parameters can be easily determined analytically, where, for instance, we can determine that the quality factor is *linearly* proportional to the length of the FPC. For an FPC with RBE, the Wigner time and LDOS are varying as  $N^2$  as calculated using asymptotic analysis [3], and  $Q$ -factor as  $N^3$ . Here we show for the first time that an FPC with DBE can enhance the total transmission gain  $G$  up to  $N^5$  for values of  $N$  ranging from a few up to  $N = 80$ , and Wigner time and LDOS scale as  $N^4$ , which is a clear and superior enhancement compared to cavities based on the RBE. These trends are determined numerically in Fig. 5(d-f) since analytical methods have not been developed yet for a photonic crystal with a DBE. Moreover, based on these observations, it can be inferred that a FPC with

DBE with smaller length can suffice to achieve even higher gain  $G$  of a much larger FPC with RBE.

## VI. CONCLUSION AND REMARKS

We have shown that the degenerate band edge (DBE) condition pertaining to an anisotropic stack of dielectric layers can be utilized to strongly enhance the gain in Fabry-Perot cavities. We have demonstrated that due to extremely large Wigner time and very high local density of states for DBE structures there is consequent giant amplification which is of orders of magnitude larger than the same obtained for uniform FPCs or for FPCs with RBE. We have also found an optimum condition for the amount of intrinsic active material that maximizes the amplification. One example of a potential application for extremely high gain is could be in Erbium doped fiber amplifiers (EDFA). High  $Q$ -factor and giant gain scaling offered by DBE structures can be utilized also in  $Q$ -switching and mode locking lasers. For instance, by varying the misalignment angles of the anisotropic layers [39], the dispersion diagram of the periodic structure can be readily altered and hence the  $Q$  factor and gain can be significantly switched [40]. Other tuning conditions can be developed with other guiding structures. These mechanisms have potential in laser applications and pulse compression optical components. DBE-based giant gain enhancement can find applications in enhancing the amplification in microwave traveling wave tubes (TWT). Indeed, our preliminary results indicate that interaction of a very low energy electron beam with electromagnetic modes in a corrugated waveguide with DBE results in extremely high amplifications. Analogous mechanisms can also be used in backward-wave-oscillator sources. In addition to that, radio frequency and microwave solid state distributed amplifiers can also benefit from using active components distributed along a microwave transmission line exhibiting the DBE.

## ACKNOWLEDGEMENT

This research was supported by AFOSR MURI Grant FA9550-12-1-0489 administered through the University of New Mexico.

## APPENDIX A: TRANSFER MATRICES OF ANISOTROPIC LAYERS

Plane wave propagation along the  $z$  direction in a dielectric described by a permittivity tensor follows the simple relation derived from Maxwell equations



$$\frac{\partial}{\partial z} \mathbf{\Psi}(z) = ik_0 \mathbf{M}(z) \mathbf{\Psi}(z), \quad (\text{A1})$$

where  $\mathbf{M}(z)$  is a  $4 \times 4$  matrix operator [10] and  $\mathbf{\Psi}(z)$  is the state-vector as in Sec. III. In the case where the dielectric is described by a symmetric relative permittivity tensor in the Cartesian coordinates reference as [10,11]

$$\begin{pmatrix} \underline{\underline{\epsilon}}(z) & 0 \\ 0 & \epsilon_{zz} \end{pmatrix}; \quad \underline{\underline{\epsilon}}(z) = \begin{pmatrix} \epsilon_{xx}(z) & \epsilon_{xy}(z) \\ \epsilon_{xy}(z) & \epsilon_{yy}(z) \end{pmatrix}, \quad (\text{A2})$$

[10,11]

an expression of the operator  $\mathbf{M}$  is given by

$$\mathbf{M}(z) = \begin{pmatrix} 0 & 0 & 0 & 1 \\ 0 & 0 & -1 & 0 \\ -\epsilon_{xy}(z) & -\epsilon_{yy}(z) & 0 & 0 \\ \epsilon_{xx}(z) & \epsilon_{xy}(z) & 0 & 0 \end{pmatrix}. \quad (\text{A3})$$

The transfer matrix described in Sec. III is then constructed from the solution of the Cauchy problem in (A1) with the appropriate boundary conditions. In short, the transfer matrix of relative to an individual layer operator  $\mathbf{M}_m$  is calculated as  $\mathbf{T}_m = \exp(i\mathbf{M}_m d_m)$  [10]. The anisotropic layers considered in this papers have parameters taken from [11],  $\epsilon_{xx} = 16.31$ ,  $\epsilon_{yy} = 5.79$  and  $\epsilon_{zz} = 1$ , however the physical concepts described in this paper are general and can be applied also to several other structures supporting two modes. The first anisotropic layer in the unit cell in Fig. 1 has an orientation  $\alpha$  of its optical axes with respect to the reference system and has  $\epsilon_{xy} = 5.26$ , whereas the second layer has an orientation  $-\alpha$ , hence it has  $\epsilon_{xy} = -5.26$ . This corresponds to a misalignment  $2\alpha$  between the two adjacent anisotropic layers of 45 degrees in the  $x$ - $y$  plane, with  $\alpha = 22.5$  degrees. The third layer in the unit cell in Fig. 1 (made of three layers) is isotropic with  $n^2 = \epsilon_{xx} = \epsilon_{yy} = \epsilon_{zz} = 1$ . When we consider an active material that leads to gain in the FPC with DBE, we consider it diluted only in the isotropic layer of each unit cell in Fig. 1. The active isotropic materials is assumed to have a refractive index equal to  $n = n' + in'' = 1 - i2.2 \times 10^{-4}$ . The same imaginary part of  $n$  is considered in one layer of the unit cell of

the FPC with RBE, i.e.,  $n_2 = 1.5 - i2.2 \times 10^{-4}$  (keeping  $n_1 = 3.2$  real). In the uniform FPC with gain in Fig. 1 we assume  $n = 2.25 - i2.2 \times 10^{-4}$ .

## APPENDIX B: CALCULATION OF THE LOCAL DENSITY OF STATES

We outline here the method we use to evaluate the local density of states through the dyadic Green's function in Cartesian coordinates for an electric sheet current in the  $x$ - $y$  plane, and located at an arbitrary point  $z'$  in a stack of anisotropic layered media shown in the inset of Fig. 1, and described by symmetric permittivity dyadic as in (A2), by generalizing the scheme used in [24,37,38] for stacks of isotropic layers. We consider a sheet current  $\mathbf{J}(z') = J_0 \hat{\mathbf{p}} \delta(z - z')$  with  $J_0$  being a constant ( $J_0$  has units of [A/m]), that is only dependent on the coordinate  $z$  and polarized along a unit vector  $\hat{\mathbf{p}}$ , where  $\hat{\mathbf{p}}$  is strictly oriented in the  $x$ - $y$  plane, i.e.,  $\hat{\mathbf{z}} \cdot \hat{\mathbf{p}} = 0$ . Consequently, only transversely polarized electromagnetic plane waves (whose electric field is orthogonal to the  $z$ -directed wavevector) are excited due to such sheet current  $\mathbf{J}(z')$ . In other words, the direction of energy flux of those propagating waves inside the stack is parallel to their wavevector, both along the  $z$ -direction. For these reasons we conveniently construct the transverse electric field response function to the Dirac delta sheet current  $\mathbf{J}(z')$ , which we identify as the  $2 \times 2$  matrix (dyadic) Green's function. First, the transverse electric field satisfies the inhomogeneous one-dimensional vector wave equation [41,42]

$$\left( \mathbf{1} \frac{\partial^2}{\partial z^2} + \underline{\underline{\epsilon}}(z) k_0^2 \right) \mathbf{E}(z, z') = -i\omega\mu_0 \mathbf{J}(z'), \quad (\text{B1})$$

where  $\mathbf{1}$  is a  $2 \times 2$  unit dyadic. Accordingly,  $2 \times 2$  matrix (dyadic) Green's function  $\underline{\underline{\mathbf{G}}}(z, z')$  is constructed by solving the following equation

$$\left( \mathbf{1} \frac{\partial^2}{\partial z^2} + k_0^2 \underline{\underline{\epsilon}}(z) \right) \underline{\underline{\mathbf{G}}}(z, z') = -\delta(z - z') \mathbf{1}, \quad (\text{B2})$$

with the appropriate boundary conditions [42,43], i.e., continuity of  $\underline{\underline{\mathbf{G}}}(z, z')$  for all values of  $z$ , the jump discontinuity in its first derivative in  $z$  due to a Dirac delta sheet current, as well as the outgoing waves

condition [24,37,38] outside the cavity in both the  $\pm z$  direction. When considering a Cartesian reference system, Green's function is a  $2 \times 2$  matrix of the form

$$\underline{\underline{\mathbf{G}}}(z, z') = \begin{pmatrix} G_{xx}(z, z') & G_{xy}(z, z') \\ G_{yx}(z, z') & G_{yy}(z, z') \end{pmatrix}. \quad (\text{B3})$$

Detailed studies of Green's functions, their properties and construction methods can be found in many mathematical physics textbooks such as Refs. [43–45], and dyadic formulations can be found in [33,41,42,46]. For our purposes we only calculate the relevant parts of the dyadic Green's function which contribute to the LDOS, as follows.

We define a projected (or partial) local density of states [33–36] pertaining to an arbitrary transverse-to- $z$  source orientation denoted by a unit vector  $\hat{\mathbf{p}}(\phi) = \cos \phi \hat{\mathbf{x}} + \sin \phi \hat{\mathbf{y}}$  where  $\phi$  spans the angular range from 0 to  $2\pi$ . This projected LDOS is proportional to the imaginary part of the Green's function and given by [35,36]

$$\rho(z, \hat{\mathbf{p}}) = -\frac{2k_0}{\pi c} \left( \text{Im} \left( \hat{\mathbf{p}} \cdot \left( \underline{\underline{\mathbf{G}}}(z, z) \cdot \hat{\mathbf{p}} \right) \right) \right). \quad (\text{B4})$$

The average of the projected LDOS over all possible orientation, as obtained in (2) is calculated as  $\rho(z) = \langle \rho(z, \hat{\mathbf{p}}) \rangle_{\hat{\mathbf{p}}}$

$$\begin{aligned} &= -\frac{k_0}{\pi^2 c} \int_0^{2\pi} \text{Im} \left( \hat{\mathbf{p}}(\phi) \cdot \left( \underline{\underline{\mathbf{G}}}(z, z) \cdot \hat{\mathbf{p}}(\phi) \right) \right) d\phi \\ &= -\frac{k_0}{\pi c} \text{Im} \left( \text{Tr} \left[ \underline{\underline{\mathbf{G}}}(z, z) \right] \right), \end{aligned} \quad (\text{B5})$$

where Tr denotes the trace. Therefore, the averaged LDOS in (2) is proportional to the trace of the imaginary part of  $\underline{\underline{\mathbf{G}}}(z, z)$  [33,36]. Therefore, instead of calculating the full dyadic Green's function, for our purpose we need to calculate only the term  $\text{Im}(G_{xx}(z, z) + G_{yy}(z, z))$ , utilizing the Poynting theorem [33,41]. For this purpose we assume a unit current sheet oriented along the  $x$ -direction, whose current density takes the form  $\mathbf{J} = \delta(z - z') \hat{\mathbf{x}}$ , for instance. The time-average power density (per-unit-area) emitted by such current sheet according to the Poynting theorem [41,42] is given by

$$\begin{aligned} P(z, \hat{\mathbf{x}}) &= -\frac{1}{2} \text{Re} \left( \int \mathbf{J}^* \cdot \mathbf{E}(z', \hat{\mathbf{x}}) dz' \right) \\ &= -\frac{1}{2} \text{Re} (E_x(z, \hat{\mathbf{x}})), \end{aligned} \quad (\text{B6})$$

where  $\text{Re}(E_x(z, \hat{\mathbf{x}}))$  is real part of the  $x$ -polarized electric field at point  $z$  due to a unit current sheet along the  $x$ -direction at the same point  $z$ . This field component is proportional to a term of dyadic Green's function in (B3) as  $\text{Im}(G_{xx}(z, z)) = \omega \mu_0 \text{Re}(E_x(z, \hat{\mathbf{x}}))$  [41,42], implying that

$$\text{Im}(G_{xx}(z, z)) = \frac{-2}{\omega \mu_0} P(z, \hat{\mathbf{x}}). \quad (\text{B7})$$

Hence calculating the power density (the right hand side of (B7)) emitted by the current sheet using the transfer matrix method allows us to compute the imaginary part of  $G_{xx}(z, z)$ . Similarly,  $\text{Im}(G_{yy}(z, z))$  is obtained by evaluating the power density emitted by a  $y$ -directed unit current sheet. The emitted power density for each of the two polarized current sources is easily calculated using the transfer matrix approach for the layered media [10–13], following Appendix A. An important consequence of (B7) is the intimate relation between the LDOS and the power emitted by the source [24,33,47]. From both (B7) and (B5) one can write the LDOS enhancement factor, which is plotted in Fig. 5(a-c), in the following form

$$\begin{aligned} \frac{\rho(z)}{\rho_{\text{free space}}} &= \frac{P(z)}{P_{\text{free space}}} \\ &= -k_0 \text{Im} (G_{xx}(z, z) + G_{yy}(z, z)), \end{aligned} \quad (\text{B8})$$

where  $P(z)$  is the emitted power density (per-unit-area) averaged over all source orientations inside the layered media.

## REFERENCES

- [1] K. Inoue, M. Sasada, J. Kawamata, K. Sakoda, and J. W. Haus, *Jpn. J. Appl. Phys.* **38**, L157 (1999).
- [2] H.-Y. Ryu, S.-H. Kwon, Y.-J. Lee, Y.-H. Lee, and J.-S. Kim, *Appl. Phys. Lett.* **80**, 3476 (2002).
- [3] J. M. Bendickson, J. P. Dowling, and M. Scalora, *Phys. Rev. E* **53**, 4107 (1996).
- [4] B.-S. Song, S. Noda, T. Asano, and Y. Akahane, *Nat. Mater.* **4**, 207 (2005).
- [5] B. Maune, M. Lončar, J. Witzens, M. Hochberg, T. Baehr-Jones, D. Psaltis, A. Scherer, and Y. Qiu, *Appl. Phys. Lett.* **85**, 360 (2004).
- [6] S. John and J. Wang, *Phys. Rev. B* **43**, 12772 (1991).

- [7] N. V. Bloch, K. Shemer, A. Shapira, R. Shiloh, I. Juwiler, and A. Arie, *Phys. Rev. Lett.* **108**, 233902 (2012).
- [8] I. Bayn, B. Meyler, A. Lahav, J. Salzman, R. Kalish, B. A. Fairchild, S. Praver, M. Barth, O. Benson, and T. Wolf, *Diam. Relat. Mater.* **20**, 937 (2011).
- [9] A. Figotin and I. Vitebskiy, *Phys. Rev. E* **68**, 036609 (2003).
- [10] A. Figotin and I. Vitebskiy, *Phys. Rev. E* **72**, 036619 (2005).
- [11] A. Figotin and I. Vitebskiy, *Phys. Rev. E* **74**, 066613 (2006).
- [12] A. Figotin and I. Vitebskiy, *Phys. Rev. A* **76**, 053839 (2007).
- [13] A. Figotin and I. Vitebskiy, *Laser Photonics Rev.* **5**, 201 (2011).
- [14] P. Yeh and C. Gu, *Optics of Liquid Crystal Displays* (John Wiley & Sons, 2010).
- [15] J. R. Burr, N. Gutman, C. Martijn de Sterke, I. Vitebskiy, and R. M. Reano, *Opt. Express* **21**, 8736 (2013).
- [16] N. Gutman, C. Martijn de Sterke, A. A. Sukhorukov, and L. C. Botten, *Phys. Rev. A* **85**, (2012).
- [17] N. Gutman, W. H. Dupree, Y. Sun, A. A. Sukhorukov, and C. M. de Sterke, *Opt. Express* **20**, 3519 (2012).
- [18] R. Colombelli, K. Srinivasan, M. Troccoli, O. Painter, C. F. Gmachl, D. M. Tennant, A. M. Sergent, D. L. Sivco, A. Y. Cho, and F. Capasso, *Science* **302**, 1374 (2003).
- [19] A. Figotin and I. Vitebskiy, *ArXiv09091393 Phys.* (2009).
- [20] J. P. Dowling, M. Scalora, M. J. Bloemer, and C. M. Bowden, *J. Appl. Phys.* **75**, 1896 (1994).
- [21] J. Grgić, J. R. Ott, F. Wang, O. Sigmund, A.-P. Jauho, J. Mørk, and N. A. Mortensen, *Phys. Rev. Lett.* **108**, 183903 (2012).
- [22] H. Ramezani, S. Kalish, I. Vitebskiy, and T. Kottos, *Phys. Rev. Lett.* **112**, 043904 (2014).
- [23] M. Fox, *Quantum Optics: An Introduction: An Introduction* (Oxford University Press, 2006).
- [24] G. D'Aguanno, N. Mattiucci, M. Scalora, M. J. Bloemer, and A. M. Zheltikov, *Phys. Rev. E* **70**, 016612 (2004).
- [25] J. T. Verdeyen, *Laser Electron.* Ed. JT Verdeyen Englewood Cliffs NJ Prentice Hall 1989 640 P **1**, (1989).
- [26] A. Yariv and P. Yeh, *Photonics: Optical Electronics in Modern Communications (The Oxford Series in Electrical and Computer Engineering)* (Oxford University Press, Inc., 2006) page.
- [27] Y. Amnon, *Quantum Electronics*, 3rd Edition (Wiley, 1989).
- [28] F. T. Smith, *Phys. Rev.* **118**, 349 (1960).
- [29] G. L. Matthaei, L. Young, and E. M. Jones, *Design of Microwave Filters, Impedance-Matching Networks, and Coupling Structures. Volume 2* (DTIC Document, 1963), page 339-350.
- [30] H. G. Winful, *New J. Phys.* **8**, 101 (2006).
- [31] T. Lauprêtre, C. Proux, R. Ghosh, S. Schwartz, F. Goldfarb, and F. Bretenaker, *Opt. Lett.* **36**, 1551 (2011).
- [32] H.-Y. Yao, N.-C. Chen, T.-H. Chang, and H. G. Winful, *Phys. Rev. A* **86**, 053832 (2012).
- [33] L. Novotny and B. Hecht, *Principles of Nano-Optics* (Cambridge university press, 2012) page 276.
- [34] A. A. Asatryan, K. Busch, R. C. McPhedran, L. C. Botten, C. Martijn de Sterke, and N. A. Nicorovici, *Phys. Rev. E* **63**, 046612 (2001).
- [35] K. Joulain, R. Carminati, J.-P. Mulet, and J.-J. Greffet, *Phys. Rev. B* **68**, 245405 (2003).
- [36] D. P. Fussell, R. C. McPhedran, and C. M. De Sterke, *Phys. Rev. E* **70**, 066608 (2004).
- [37] O. D. Stefano, S. Savasta, and R. Girlanda, *J. Mod. Opt.* **48**, 67 (2001).
- [38] G. D'Aguanno, M. Centini, M. Scalora, C. Sibilia, M. Bertolotti, M. J. Bloemer, and C. M. Bowden, *JOSA B* **19**, 2111 (2002).
- [39] K.-Y. Jung and F. L. Teixeira, *Phys. Rev. B* **77**, 125108 (2008).
- [40] V. A. Tamma, A. Figotin, and F. Capolino, *ArXiv13107645 Phys.* (2013).
- [41] R. E. Collin, *Field Theory of Guided Waves* (Wiley-IEEE Press, 1991) page 121-134.
- [42] J. G. Van Bladel, *Electromagnetic Fields* (John Wiley & Sons, 2007), page 1035-1042.
- [43] P. Dennery and A. Krzywicki, *Mathematics for Physicists* (Courier Dover Publications, 1996).
- [44] B. Friedman, *Principles and Techniques of Applied Mathematics* (New York, 1961).
- [45] R. Courant and D. Hilbert, *Methods of Mathematical Physics* (CUP Archive, 1966) page 351-286.
- [46] C.-T. Tai, *Dyadic Green Functions in Electromagnetic Theory* (IEEE press New York, 1994).
- [47] X. Liang and S. G. Johnson, *Opt. Express* **21**, 30812 (2013).